processes

MDPI

Article

Nano Zero-Valent Iron (nZVI) Encapsulated with ABS (nZVI/(ABS + EC)) for Sustainable Denitrification Performance and Anti-Aggregation

Fanbin Meng [1,2], Yuning Yang [1], Miao Li [2,*], Qizhi Zhu [1], Bing Qin [1] and Chunpeng Yang [1]

[1] SINOPEC Research Institute of Petroleum Processing Co., Ltd., Beijing 100083, China; mfb1469@163.com (F.M.); qinbing.ripp@sinopec.com (B.Q.); yangchunpeng.ripp@sinopec.com (C.Y.)
[2] School of Environment, Tsinghua University, Beijing 100084, China
* Correspondence: miaoli@tsinghua.edu.cn

Abstract: Aggregation and sharp reactivity decrease are the key problems of using nano zero-valent iron (nZVI) as a potential reaction medium for a permeable reactive barrier (PRB). In this study, nZVI particles encapsulated within an acrylonitrile–butadiene–styrene (ABS) matrix (nZVI/(ABS + EC)) was fabricated, which for the first time successfully simultaneously solved the above problems via accurately regulating the distribution of nZVI particles in the ABS matrix and regulating the contact between nZVI particles and the contaminated aqueous environment. In addition, the size and number of the pores throughout the ABS matrix were first regulated by ethyl cellulose (EC) for the purpose of controlling the contact between nZVI particles and the nitrate contaminant, affording apparent rate constants (k_{obs}) for denitrification performance in the range of 0.0423 to 0.0820 min^{-1}. The remediation of simulated nitrate-contaminated solution by nZVI/(ABS + EC) was suitably described by the first-order kinetics model, with k_{obs} ranging from 0.0423 to 0.2036 min^{-1}, and functional relationship models of k_{obs} with the dosages of EC (d_{EC}) and nZVI (d_{Fe}) during encapsulation were developed for the quantitative regulation of a sustainable denitrification performance. Results revealed that encapsulation prevents the aggregation of nZVI, rendering a sustainable denitrification performance of the material; the denitrification performance was demonstrated to be affected and quantitatively regulated by the encapsulation and application conditions. Using nZVI/(ABS + EC) as the reaction medium for PRB, the pore blocking of PRB can be avoided, and the sustainable remediation performance can be quantitatively regulated and predicted.

Keywords: nano zero-valent iron; permeable reactive barrier; denitrification performance; aggregation; reactivity decrease

Citation: Meng, F.; Yang, Y.; Li, M.; Zhu, Q.; Qin, B.; Yang, C. Nano Zero-Valent Iron (nZVI) Encapsulated with ABS (nZVI/(ABS + EC)) for Sustainable Denitrification Performance and Anti-Aggregation. *Processes* **2024**, *12*, 697. https://doi.org/10.3390/pr12040697

Academic Editor: Andrea Petrella

Received: 11 March 2024
Revised: 26 March 2024
Accepted: 27 March 2024
Published: 29 March 2024

1. Introduction

Nitrate is a pervasive and typical groundwater contaminant [1] originating from sources like industrial and domestic waste [2], extensive use of fertilizers [3], and emissions of animal dung [4]. Moreover, the consumption of nitrate-contaminated groundwater can increase the risk of gastric and esophageal cancers and lead to methemoglobinemia in babies [5,6].

As the key technology for the in situ remediation of nitrate-contaminated groundwater, currently, permeable reactive barrier (PRB) remediation systems mainly use highly reductive, cost-effective zero-valent iron (ZVI) as the reaction medium [7,8]. Owing to its high specific surface area, nZVI exhibits a high reactivity and contamination removal rate. A kinetics study revealed that the reduction rate of nitrate by nZVI is 10 to 100 times more rapid than that of micro-scale iron particles [9–11]. Hence, PRB using nZVI as the reaction medium exhibits an advantage for the removal rate of the contaminant and elimination of the pollutants at high concentrations. In view of the rapid development of nanotechnology

and considerable potential advantages of nZVI, experiments and applications using nZVI as the reaction medium for PRB have been performed by several researchers [12–14].

However, aggregation [15,16] and poor reactivity persistence [17] are the bottleneck issues in the use of nZVI as a reaction medium for PRB [18,19]. Hence, several studies [20,21] have been extensively conducted to overcome these bottleneck issues. The encapsulation of nZVI particles in a porous matrix is a typical approach to immobilize nZVI particles and ultimately prevent aggregation [22]. Calcium alginate beads constitute one of the typical encapsulation materials, and these beads have been used to immobilize nZVI particles [23,24]. Encapsulated nZVI particles can contact and react with contaminants via holes throughout the calcium alginate beads. In addition to calcium alginate, polystyrene (PS) [25], chitosan [26], and carbon spheres [27,28] have been used to prevent the aggregation of nZVI particles.

To increase the reactivity persistence of nZVI, several strategies [20,21] have been developed to extend its reactivity period. The most sophisticated method to improve the longevity of nZVI is to emulsify nZVI particles with vegetable oil and other additives to decrease their corrosion rate [29]. The emulsification of nZVI considerably increases its longevity by restraining the contact between nZVI particles and the contaminant [21]; however, owing to its good flow behavior, nZVI emulsified with vegetable oil is only suitable for in situ remediation and not for PRB remediation. Complicated hydrogeology may have resulted in the destabilization of the nZVI and vegetable oil suspension, ultimately leading to aggregation. Generally, previous studies have focused on solving either the aggregation or poor reactivity persistence; however, few studies on synchronously solving both aggregation and poor reactivity persistence have been conducted, and studies on the quantitative regulation of the nZVI reactivity persistence have not been conducted.

Synchronously solving both aggregation and poor reactivity persistence constitutes the core issue for using nZVI as the reactive medium for PRB; therefore, the key technology is to synchronously implement the immobilization of nZVI particles and control the contact between the nZVI particles and contaminant. Encapsulation is typically employed to stabilize active ingredients in drug delivery [30–33], pesticides [34–37], self-healing [38], and food [39–41]. However, current studies [42] devoted to the use of nZVI as an alternative reactive media for PRB have mostly focused on the use of encapsulation for immobilizing nZVI to prevent aggregation. Encapsulation has been rarely applied to improve the longevity of nZVI, and attempts have not been made to employ encapsulation to simultaneously reduce aggregation and prevent the sharp reactivity loss of nZVI to the best of our knowledge. The ability of encapsulation to immobilize nZVI and prevent aggregation has been demonstrated by previous studies. Previous studies have reported that encapsulation can enable the sustainable release of reactive nZVI and ultimately maintain its continuous reactivity. Hence, encapsulation is feasible to simultaneously prevent aggregation and increase the reactivity persistence of nZVI.

However, to the best of our knowledge, studies have not been conducted to employ the encapsulation for the synchronous solution of aggregation and sharp reactivity decrease in nZVI and to quantitatively regulate the reactivity persistence of nZVI. Hence, this study explores the encapsulation of nZVI particles into an acrylonitrile–butadiene–styrene (ABS) matrix to immobilize nZVI particles. In addition, different dosages of ethyl cellulose (EC) were used to modify the pores throughout the ABS matrix to regulate the size and number of holes and further control the contact between nZVI particles and the contaminant. Moreover, the apparent rate coefficient (k_{obs}) for nitrate removal using encapsulated nZVI was calculated by numerical simulations by utilizing different dosages of EC and Fe^0 based on batch experiments. In addition, effects of the morphology, structure, and denitrification conditions on the denitrification performance of nZVI encapsulated in ABS were thoroughly investigated.

2. Experimental

2.1. Materials and Methods

ABS (industrial grade, M_w = 10,000–12,000) was provided by Langfang Juxin Plastic Factory (Langfang, China). Both ethyl cellulose (EC) and polyvinyl pyriloxanone (PVP, K30) were supplied by Sinopharm Chemical Reagent Co., Ltd. (Beijing, China). Ferrous sulfate ($FeSO_4 \bullet 7H_2O$, >99%) was purchased from Fuchen (Tianjin) Chemical Reagent Co., Ltd. (Tianjin, China) Methylene dichloride (CH_2Cl_2, >98%), ethanol (CH_3CH_2OH, >99.7%), and n-heptane were purchased from Beijing Chemical Works (Beijing, China). Sodium borohydride ($NaBH_4$, >99%) was producted by Shanghai Aladdin Biochemical Technology Co., Ltd. (Shanghai, China). Polydimethylsiloxane (PDMS, commercial grade, 3000 cSt) were obtained from Dow Coring XIAMETER® (DeLand, FL, USA). All reagents were used as received. Deionized water was used throughout this research and was deoxygenated before use.

In this study, reagent-grade $NaNO_3$, which was purchased from Sinopharm Chemical Reagent Co., Ltd. (Beijing, China), was chosen as the target compound. The simulated pollutant solution with different NO_3^--N concentrations were prepared by dissolving specified amounts of $NaNO_3$ in deoxygenated water.

To monitor the denitrification performance of the following samples, 0.5 mL aliquots were extracted at various reaction times. Then, they were diluted to 25.0 mL to analyze the NO_3^--N concentrations using ultraviolet spectrophotometry (HACH DR6000, HACH, Loveland, CO, USA) at the absorbance wavelengths of 220 and 275 nm.

2.2. The nZVI Preparation

The synthesis of nZVI was carried out by a classical liquid phase reduction method. At room temperature (25 °C), 0.50 g of PVP was added to a $FeSO_4 \bullet 7H_2O$ solution (50 mL, 0.01 mol/L) and stirred by a mechanical agitator at a rate of 200 r/min. After 20 min, the PVP was completely dissolved, and then 50 mL of $NaBH_4$ solution (0.03 mol/L) was poured into the above mixed solution of $FeSO_4 \bullet 7H_2O$ and PVP. After 10 min, the generated Nzvi particles were collected via magnetic separation. Finally, the obtained Nzvi particles were washed three times with 100 mL of ethanol, and then dried at 60 °C using a vacuum drying oven (DHG-9005, Yi Heng, Shanghai, China).

2.3. Encapsulation of Nzvi Particles

First, the shell material solution was prepared by dissolving 0.25 g of ABS and the desired weight of EC into 30 mL of methylene dichloride in a 100 mL three-neck round-bottom flask under 200 r/min stirring. After that, the synthesized Nzvi particles were added into the above shell material solution. After 10 min, the nZVI particles were successfully suspended in the shell material solution, and then 30 mL of PDMS was added dropwise into the above suspension to induce the coacervation of ABS and EC. After titration, the mixture in the three-neck round-bottom flask was poured into 250 mL of n-heptane to solidify the shell, and the obtained particles were also collected via magnetic separation. The collected particles were washed three times with 100 mL of n-heptane, and then soaked in 50 mL of ethanol for 24 h to remove EC. Finally, the particles were separated from the ethanol and dried at 60 °C in a vacuum drying oven for 6 h, and the obtained sample was named nZVI/(ABS + EC). In addition, the parameter conditions and nomenclature for the samples prepared in this study are shown in Table 1.

Table 1. Nomenclature for nZVI/(ABS + EC) samples fabricated under various encapsulation conditions.

Sample No.	m (ABS)	m (EC)	m (nZVI)	Nomenclature
1	0.25	0.15	0.15	nZVI/(ABS + EC) - (0.6–0.6)
2	0.25	0.15	0.20	nZVI/(ABS + EC) - (0.6–0.8)
3	0.25	0.15	0.25	nZVI/(ABS + EC) - (0.6–1.0)
4	0.25	0.15	0.50	nZVI/(ABS + EC) - (0.6–2.0)
5	0.25	0.00	0.25	nZVI/ABS
6	0.25	0.02	0.25	nZVI/(ABS + EC) - (0.08–1.0)
7	0.25	0.05	0.25	nZVI/(ABS + EC) - (0.2–1.0)
8	0.25	0.10	0.25	nZVI/(ABS + EC) - (0.4–1.0)
9	0.25	0.20	0.25	nZVI/(ABS + EC) - (0.8–1.0)
10	0.25	0	0	ABS

2.4. Characterization of the nZVI/(ABS + EC)

SEM:

Scanning electron microscopy (SEM, ZEISS Merlin, Oberkochen, Germany) was used to observe the morphology of the ABS-encapsulated nZVI, the virgin nZVI/(ABS + EC) - (0.6–0.8), and nZVI/(ABS + EC) - (0.6–0.8) after the denitrification reaction. Also, morphology changes in the ABS and EC composites after immersion in ethanol were observed by SEM to verify the fabrication mechanism of nZVI/(ABS + EC). Finally, nZVI/(ABS + EC) - (0.6–0.8) was deironized after the deironization by immersion in the hydrochloric acid solution (0.1 mol/L, 50 mL) for 48 h and then the matrix morphology of nZVI/(ABS + EC) was observed by SEM.

BET:

The specific surface area, total pore volume and porosity of the nZVI/ABS, nZVI/(ABS + EC) without alcoholic impregnation, and nZVI/(ABS + EC) after alcoholic impregnation were measured by a BET-surface area analyzer (Quantachrome Instruments, America), and calculated by the Brunauer–Emmett–Teller (BET) and Barrett–Joyner–Halenda (BJH) models from the N_2 adsorption isotherms.

Batch experiment:

Batch experiments were carried out to determine the influence of preparation and denitrification conditions on the denitrification performance of nZVI/(ABS + EC). A comparison experiment using nZVI and ABS as the denitrification agent was also conducted. All batch experiments were conducted in 50 mL glass bottles under an anaerobic environment, and the reaction temperature was controlled by a water bath (HH-8 Kexi, Kexi Co. Ltd., Beijing, China). To create an anaerobic environment for our denitrification experiments, upon addition of nZVI/(ABS + EC) to glass bottles containing the simulated pollutant solution, the bottles were promptly sealed with aluminum caps and rubber stoppers to prevent air ingress. Sampling at predetermined time intervals was conducted by penetrating the rubber stopper with a syringe to extract 0.5 mL of sample, ensuring the maintenance of anaerobic conditions throughout the nitrate removal process.

The effects of EC and nZVI dosage during preparation on the denitrification performance of encapsulated nZVI were studied. The remediation of a solution of 50 mg/L NO_3^--N (25 mL) was conducted using 0.1 g of nZVI/(ABS + EC) fabricated with various EC and nZVI dosages at 25 °C and an unregulated initial pH.

The factors for the NO_3^--N removal by nZVI/(ABS + EC) were investigated by remediating a NO_3^--N solution (25 mL) at 25 °C, using nZVI/(ABS + EC) - (0.6–0.8) as the reductant to remove nitrate.

(1) The initial pH of the system

Batch experiments were conducted at pH values of 3, 5, 7, 9, and 11 with an nZVI/(ABS + EC) - (0.6–0.8) dosage of 4 g/L and an initial NO_3^--N concentration of 50 mg/L.

(2) The initial NO_3^--N concentration

Batch experiments were conducted at initial NO_3^--N concentrations (c_0) of 15 mg/L, 25 mg/L, 50 mg/L, 75 mg/L, and 100 mg/L with an nZVI/(ABS + EC) - (0.6–0.8) dosage of 4 g/L without controlling the initial pH.

(3) The reductant concentration

Batch experiments were conducted at initial reductant concentrations of 2 g/L, 4 g/L, 6 g/L, and 8 g/L with an NO_3^--N concentration of 50 mg/L and an uncontrolled initial pH.

In this study, based on the results of the above batch experiments, the denitrification kinetics by nZVI/(ABS + EC) under various preparation conditions and denitrification conditions were investigated by developing an *n*th-order reaction model (Equation (1)).

$$r = -\frac{d\left[NO_3^-\right]}{dt} = k_{obs}\left[NO_3^-\right]^n \quad (1)$$

where k_{obs} is the observed *n*th-order reaction rate constant. The total duration of each set of experiments was extended to 48 h to comprehensively assess the nitrate removal capability of nZVI/(ABS + EC) over a broad range of operational conditions. However, detailed observations and data analysis focused on the initial 24 h, during which the most significant nitrate removal was observed, highlighting the rapid effectiveness of the nZVI/(ABS + EC) system in reducing NO_3^--N concentrations.

3. Results and Discussion

3.1. nZVI and Matrix Modification Mechanism

The SEM images in Figure 1 show that the obtained Fe^0 particles were 70 nm and spherical in shape. Obvious aggregation of nZVI particles appeared on the SEM image. What is worse, the aggregation of nZVI particles deteriorated during the denitrification process for the Fe^0 corrosion reaction. ABS was used to encapsulate water-soluble core materials (such as oxalic acid [43], potassium persulate [44]) for sustainable release performance. Some small holes appeared on the surface of the ABS matrix, which can significantly affect the nZVI release rate. Moreover, the surface appearance of the ABS and EC composite matrix was similar to that of ABS (Figure 1b,c).

However, both the nZVI encapsulated with ABS and the composite of ABS and EC exhibited very slow denitrification rates. The primary analysis suggests that the size and number of pores influenced the denitrification rate, and these pores may have been produced by the ethanol impregnation process of the ABS and EC composite (Figure 2). After impregnation, more and larger holes appeared on the surface of the ABS and EC composite matrix (Figure 2d). It can be inferred that the size and number of the pores was controlled by the EC content of the composite.

3.2. Morphology Observation

After alcoholic impregnation, many pores were exposed on the matrix surface, and a mass of catenaries constituted by nZVI particles appeared on the pore walls (Figure 3a,b). The nZVI particles spread on the pore wall could limit particle movement and ultimately prevent nZVI nanoparticle aggregation. After deironization via immersion in dilute HCl solution, many more pores were observed in the nZVI/(ABS + EC) - (0.6–1.0) (Figure 3c), which may have been caused by the removal of nZVI particles embedded in nZVI/(ABS + EC) - (0.6–1.0). Also, the morphology of the nZVI/(ABS + EC) - (0.6–1.0) after denitrification was observed by SEM, which showed that a number of irregularly-shaped particles were attached to the surface and pore wall (Figure 3d), which could impede the contact of the nZVI particles and contaminants. Therefore, it can be inferred from the obtained SEM images that a large number of pores was produced by the fabrication method, and the nZVI particles were successfully supported on the pore walls or were embedded within the matrix. However, the deposition of iron oxides generated from the denitrification reaction may adversely affect the denitrification rate.

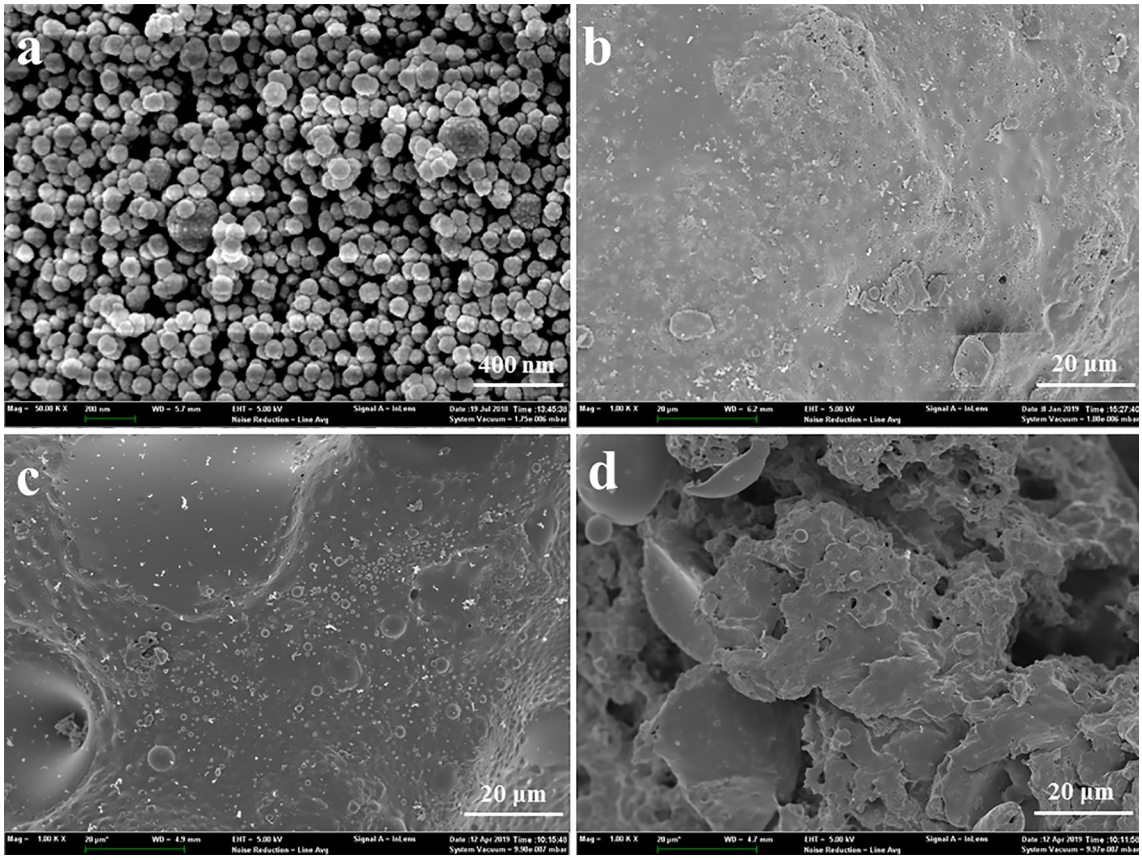

Figure 1. SEM images of nZVI (**a**), ABS matrix (**b**), the matrix of the ABS and EC composite (**c**), and the matrix of the ABS and EC composite after ethanol impregnation (**d**).

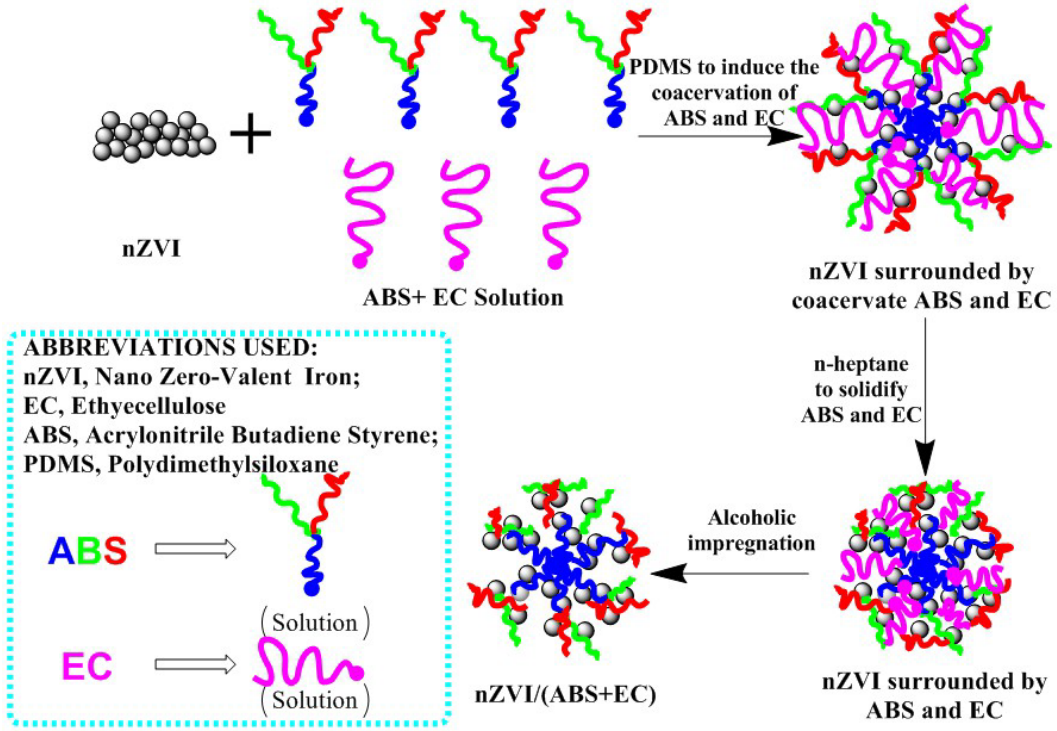

Figure 2. The encapsulation mechanism of nZVI in the ABS matrix via coacervation induced by PDMS.

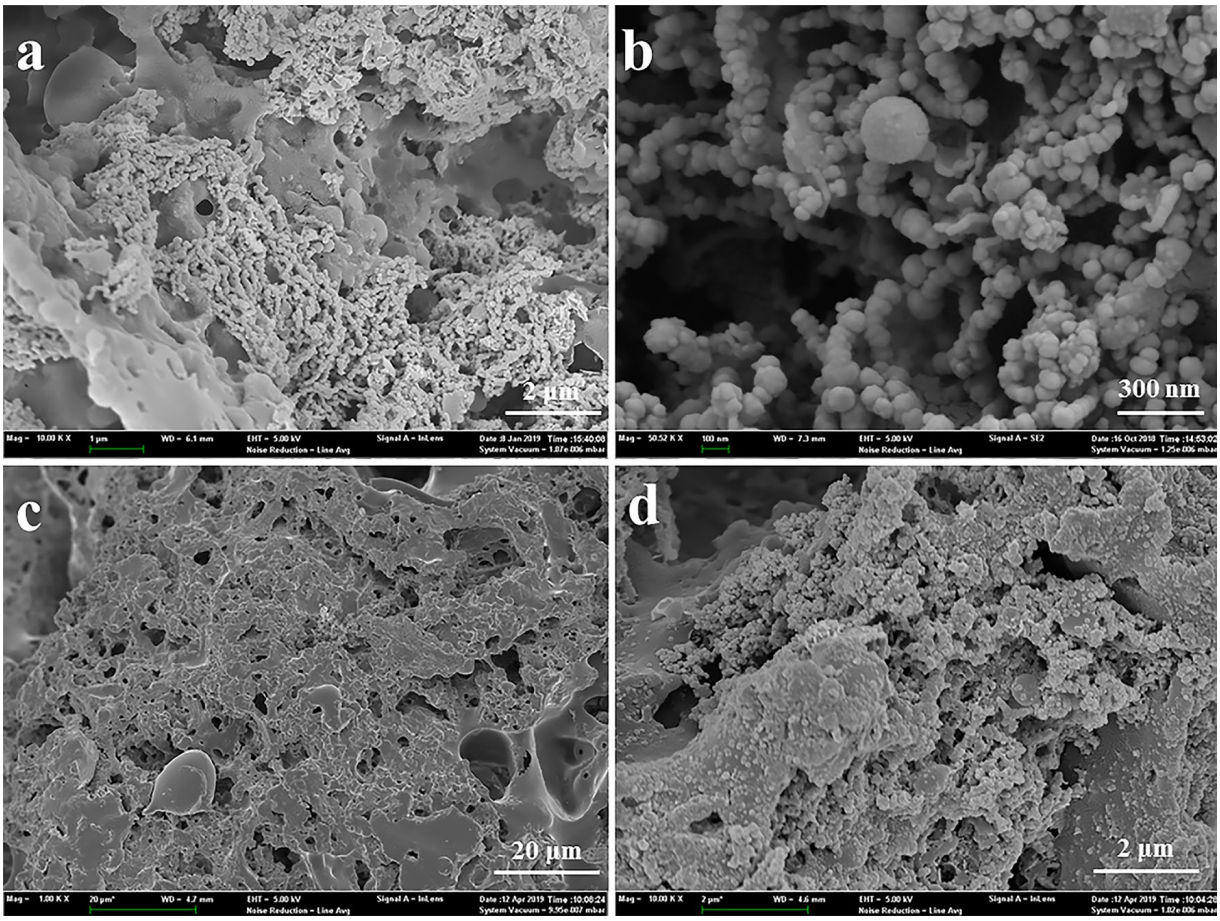

Figure 3. SEM images of nZVI/(ABS + EC) - (0.6–1.0) (**a**,**b**), nZVI/(ABS + EC) - (0.6–1.0) after the deironization (**c**), and nZVI/(ABS + EC) - (0.6–1.0) (**a**,**b**) after denitrification (**d**).

3.3. BET Test

All N_2 adsorption/desorption isotherms of nZVI/ABS, nZVI/(ABS + EC) without alcoholic impregnation, and nZVI/(ABS + EC) after alcoholic impregnation displayed a typical type IV isotherm (IUPAC classification) with an H3 hysteresis loop (Figure 4). These results indicate the mesoporous and macroporous structures of all samples. This is also supported by the pore size distribution (Figure 4 inset image), which shows that the nZVI/(ABS + EC) after alcoholic impregnation was dominated by many small holes with a diameter greater than 15 nm. In addition, the pore volumes of nZVI/ABS, nZVI/(ABS + EC) without alcoholic impregnation, and nZVI/(ABS + EC) after alcoholic impregnation were 0.074, 0.071, and 0.130 cc/g, respectively. The obtained BET results confirm that the holes in the matrix were formed due to alcoholic impregnation, which agrees with the SEM observations. Therefore, it can be inferred that the alcoholic impregnation process can be used to achieve the sustained release of nZVI encapsulated by an ABS and EC composite.

3.4. Effects of EC Dosage

The ABS particles showed almost no removal effect on nitrate, moreover, the denitrification rates of all encapsulated nZVI samples were notably lower than that of bare nZVI (Figure 5a), indicating that the ABS alone had negligible effects on nitrate reduction, but the encapsulation with ABS enabled sustainable denitrification. The maximum adsorption capacity of nZVI prepared in this study for nitrate was as high as 142.952 mg/g (m_N/m_{nZVI}). However, compared to nZVI/(ABS + EC) samples, nZVI exhibited extremely fast denitrification rates (Figure 5a), indicating that encapsulation enabled sustainable denitrification. The obtained results (Table 2) indicate a first-order dependence of denitrification on EC dosage

during encapsulation. Moreover, k_{obs} increased as d_{EC} increased, which was attributed to a higher number of holes in the matrix (Figure 5b). The number of holes was affected by the EC dosage during encapsulation, which further influenced the denitrification rate of the encapsulated nZVI. For denitrification at an initial NO_3^--N concentration of 50 mg/L, with a dosage of 0.10 g encapsulated nZVI, the functional relationship between k_{obs} and d_{EC} is given as follows (Equation (2)):

$$k_{obs} = -0.7463 \times {d_{EC}}^2 + 0.3898 \times d_{EC} + 0.0342 \quad (2)$$

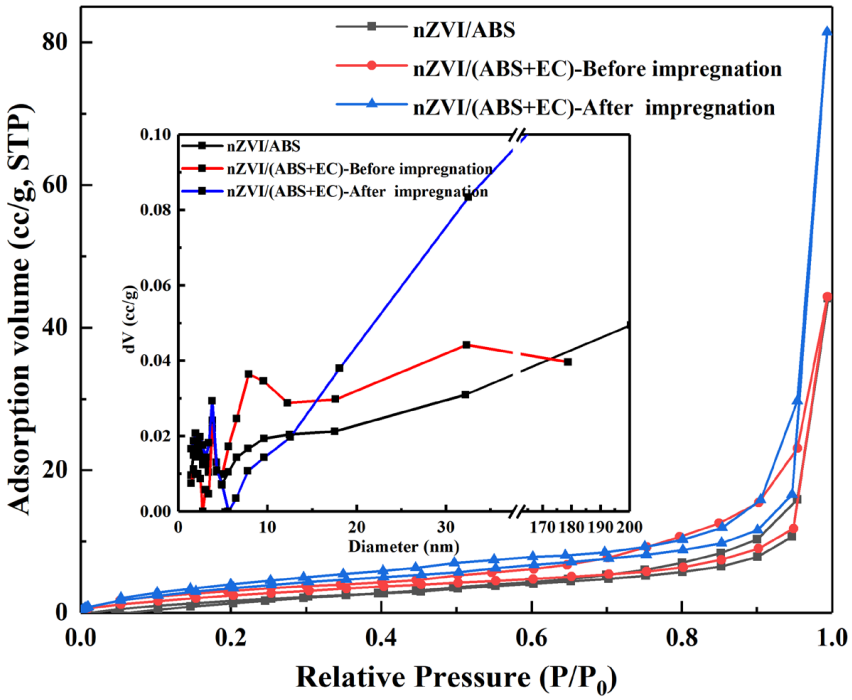

Figure 4. The N_2 adsorption/desorption isotherm and BJH (Barrett–Joyner–Halenda) pore size distribution (inset) of nZVI/ABS, nZVI/(ABS + EC) without alcoholic impregnation, and nZVI/(ABS + EC) after alcoholic impregnation.

Table 2. The k_{obs} of samples prepared with different EC dosages during encapsulation.

Sample	d_{EC}	k_{obs}/min^{-1}	R^2
nZVI/(ABS + EC) - (0.08–1.0)	0.02	0.0423	0.9500
nZVI/(ABS + EC) - (0.2–1.0)	0.05	0.0507	0.9304
nZVI/(ABS + EC) - (0.4–1.0)	0.10	0.0659	0.9385
nZVI/(ABS + EC) - (0.6–1.0)	0.15	0.0763	0.8805
nZVI/(ABS + EC) - (0.8–1.0)	0.20	0.0820	0.8695

This outcome reinforces our hypothesis that the observed denitrification is primarily attributable to the activity of nZVI. Therefore, it can be concluded that the EC dosage during encapsulation was an important parameter influencing the denitrification rate when encapsulated nZVI was used to reduce nitrate. The sustainable denitrification rate can be quantitatively regulated by the EC dosage during encapsulation.

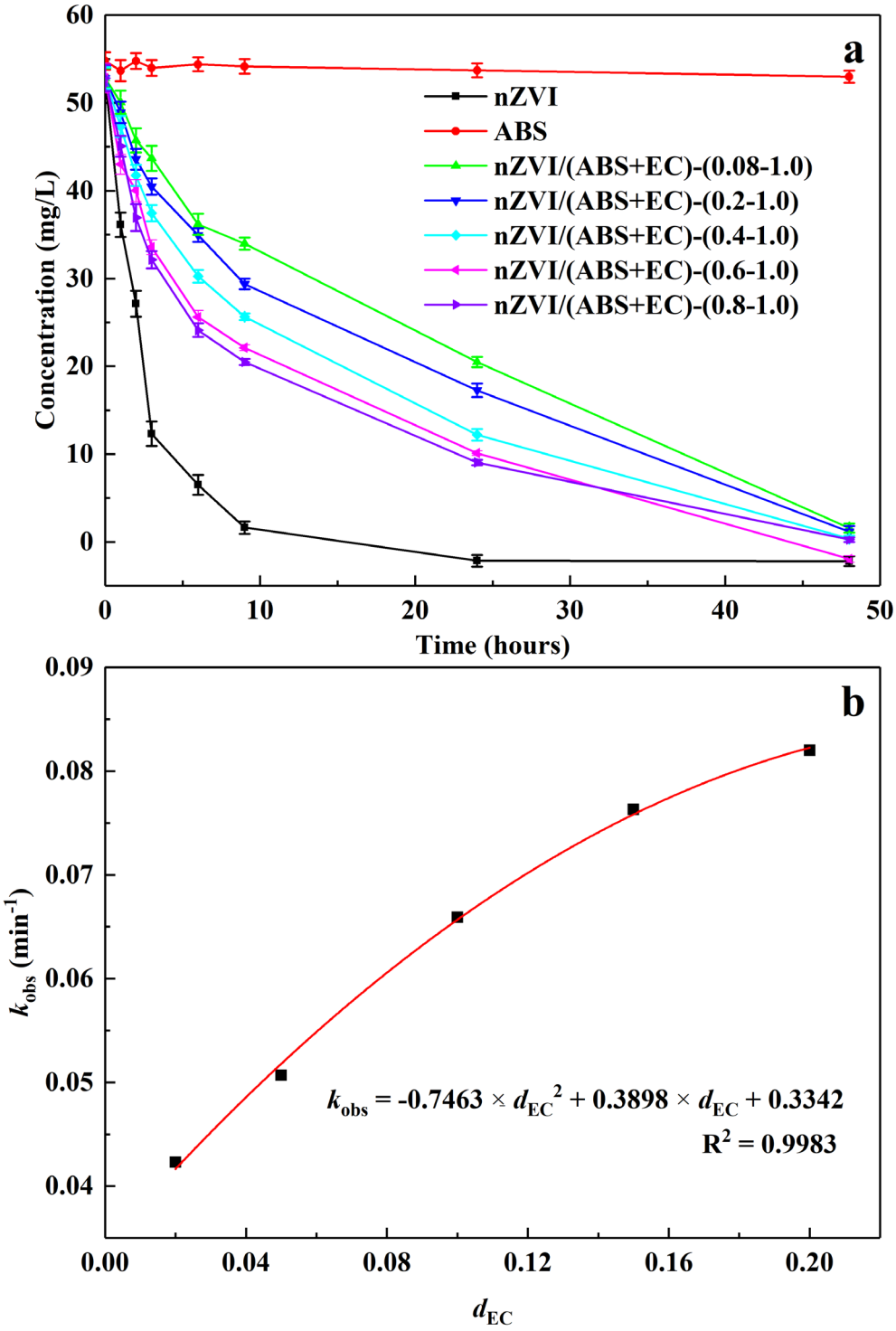

Figure 5. The denitrification performance (**a**) and k_{obs} (**b**) of nZVI and samples prepared under different EC dosages during encapsulation.

3.5. Effects of nZVI Dosage

The encapsulated nZVI samples had an obvious sustainable denitrification effect, and the denitrification rate of encapsulated nZVI was affected by the nZVI dosage (d_{Fe}) during encapsulation (Figure 6a). A linear model closely fit the data (Table 3, $R^2 \geq 0.9902$ in all cases), demonstrating that the reaction was first order with respect to the nZVI dosage

during encapsulation. Also, k_{obs} increased with d_{Fe} (Figure 6b), and the calculation of k_{obs} can be expressed by the following equation (Equation (3)):

$$k_{obs} = -0.3128 \times {d_{Fe}}^2 + 0.5361 \times d_{Fe} + 0.014 \quad (3)$$

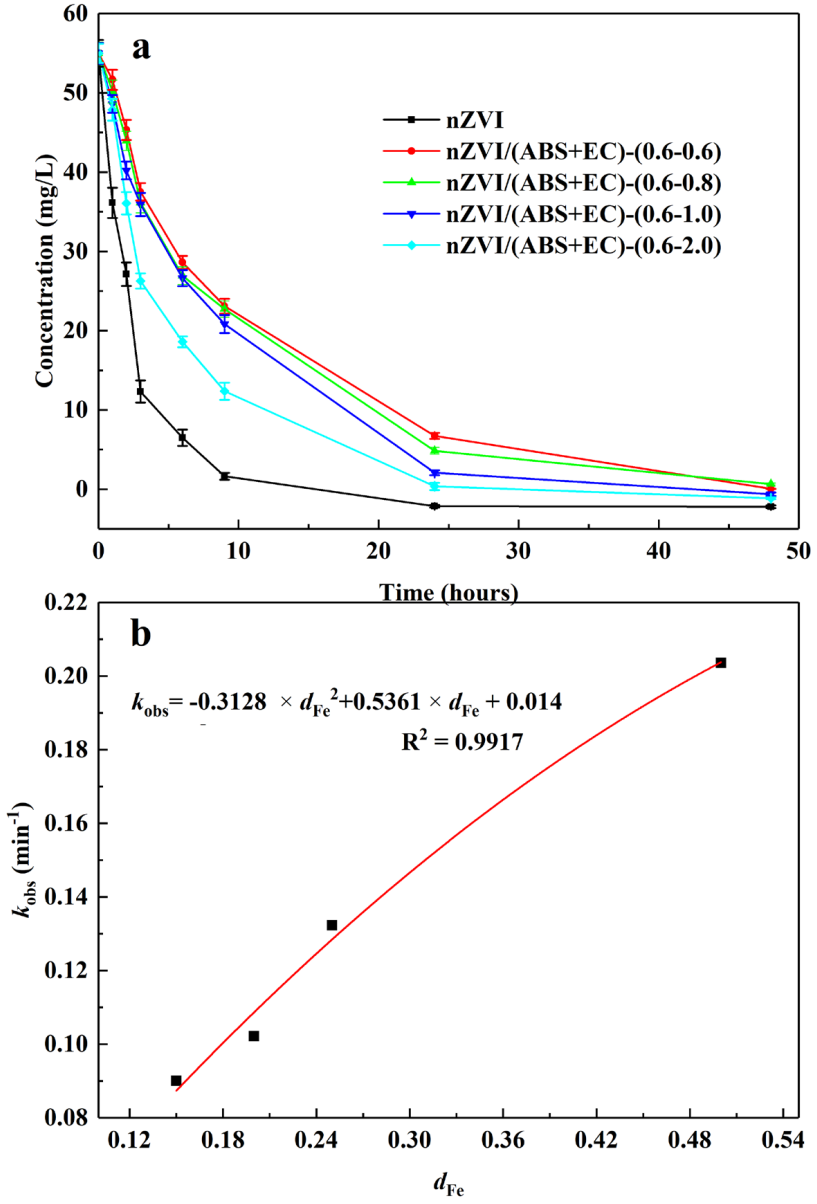

Figure 6. The denitrification performance (**a**) and k_{obs} (**b**) of nZVI and samples prepared under different nZVI dosages during encapsulation.

Table 3. The k_{obs} of samples prepared under different nZVI dosages during encapsulation.

Sample	d_{Fe}	k_{obs}/min^{-1}	R^2
nZVI/(ABS + EC) - (0.6–0.6)	0.15	0.0901	0.9895
nZVI/(ABS + EC) - (0.6–0.8)	0.20	0.1022	0.9939
nZVI/(ABS + EC) - (0.6–1.0)	0.25	0.1323	0.9914
nZVI/(ABS + EC) - (0.6–2.0)	0.50	0.2036	0.9902

The above results indicate that, in addition to the EC dosage during encapsulation, the nZVI dosage significantly influenced the denitrification rate. Thus, adjusting

the nZVI dosage during encapsulation is a feasible method to regulate the sustainable denitrification rate.

3.6. Effects of pH

When the initial pH ranged from 3 to 11, nZVI/(ABS + EC) - (0.6–0.8) presented a fast denitrification rate with some differences (Figure 7), and the effect of pH on the denitrification rate was highly variable. The fastest denitrification rates were observed at initial pH values of 3 and 9. The slowest denitrification rate was observed at the early stage of the reaction at an initial pH of 5, and also during the later reaction stage at an initial pH of 11. To explain the above phenomena, it is necessary to examine the denitrification mechanisms of Fe^0 proposed by Xu [45].

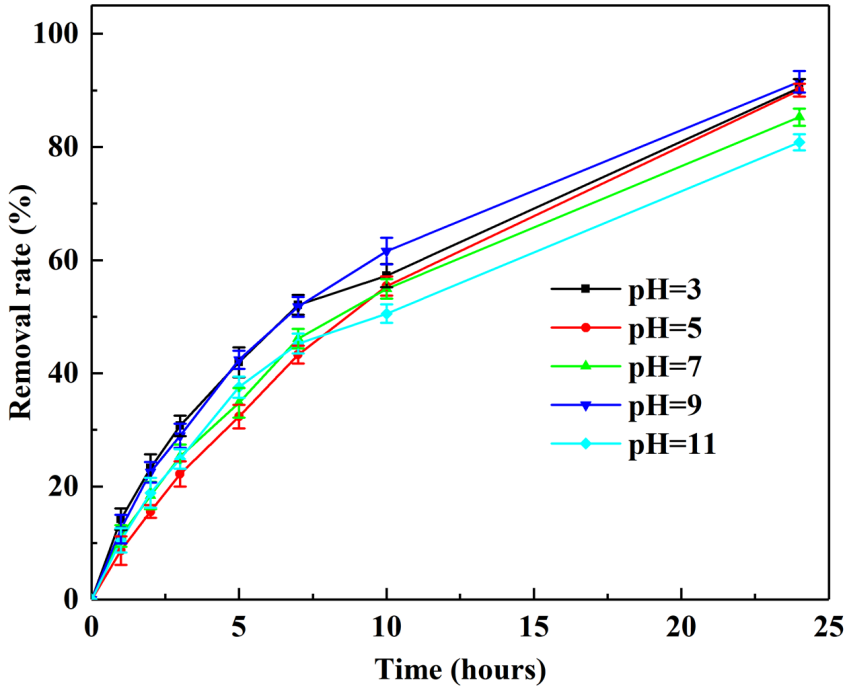

Figure 7. The influence of pH on the denitrification performance of nZVI/(ABS + EC) - (0.6–0.8).

Primarily, the reduction of nitrate occurs due to an electron provided by Fe^0 (Equations (4) and (5)).

$$Fe^0 \rightarrow Fe^{2+} + 2e^- \quad (4)$$

$$NO_3^- + 10H^+ + 8e^- \rightarrow NH_4^+ + 3H_2O \quad (5)$$

When the concentration of H^+ in the system was low, the nitrate reduction rate decreased, accompanied by the generation of Fe_3O_4 (Equations (6) and (7)).

$$3Fe^0 + 3H_2O \rightarrow Fe_3O_4 + 8H^+ + 8e^- \quad (6)$$

$$3Fe^{2+} + 4H_2O + 8e^- \rightarrow Fe_3O_4 + 8H^+ + 2e^- \quad (7)$$

The corrosion of the iron surface would supply electrons for nitrate reduction. The generated Fe_3O_4 is a good conductor for electron transfer and eventually increased the nitrate removal rate. However, corrosion and Fe_3O_4 deposition on the iron surface were significantly influenced by the system pH. An acidic pH accelerated the iron surface corrosion and increased the nitrate removal rate at a pH of 3. When the system was under weakly basic conditions, Fe_3O_4 was easily generated, and the denitrification rate was also fast at a pH of 9. However, to explain the nitrate removal performance of the encapsulated nZVI between pH values from 5 to 7, the contribution of corrosion and Fe_3O_4 deposition to nitrate removal should be quantitatively evaluated. The above results indicate that

encapsulated nZVI could rapidly remove nitrate between pH values from 3 to 11, and the pH of the reducing system was not significant, but it had a complicated effect on the denitrification rate.

3.7. Effects of Initial Nitrate Concentration

Previous studies have confirmed that the initial NO_3^--N concentration is intimately related to the denitrification rate of nZVI. However, Wang et al. [46] reported that the denitrification rate of nZVI decreased with the initial NO_3^--N concentration, but Yang et al. [10] reported the opposite. Moreover, encapsulated nZVI showed complicated denitrification performance at different initial NO_3^--N concentrations (Figure 8a). In this study, the nitrate reduction by nZVI/(ABS + EC) - (0.6–0.8) at different initial NO_3^--N concentrations is described by a first-order kinetic model (Table 4). However, the impact of the initial NO_3^--N concentration on k_{obs} was not monotonic (Figure 8b), and the reported relevant literatures has not reached a consensus on this issue [10,47].

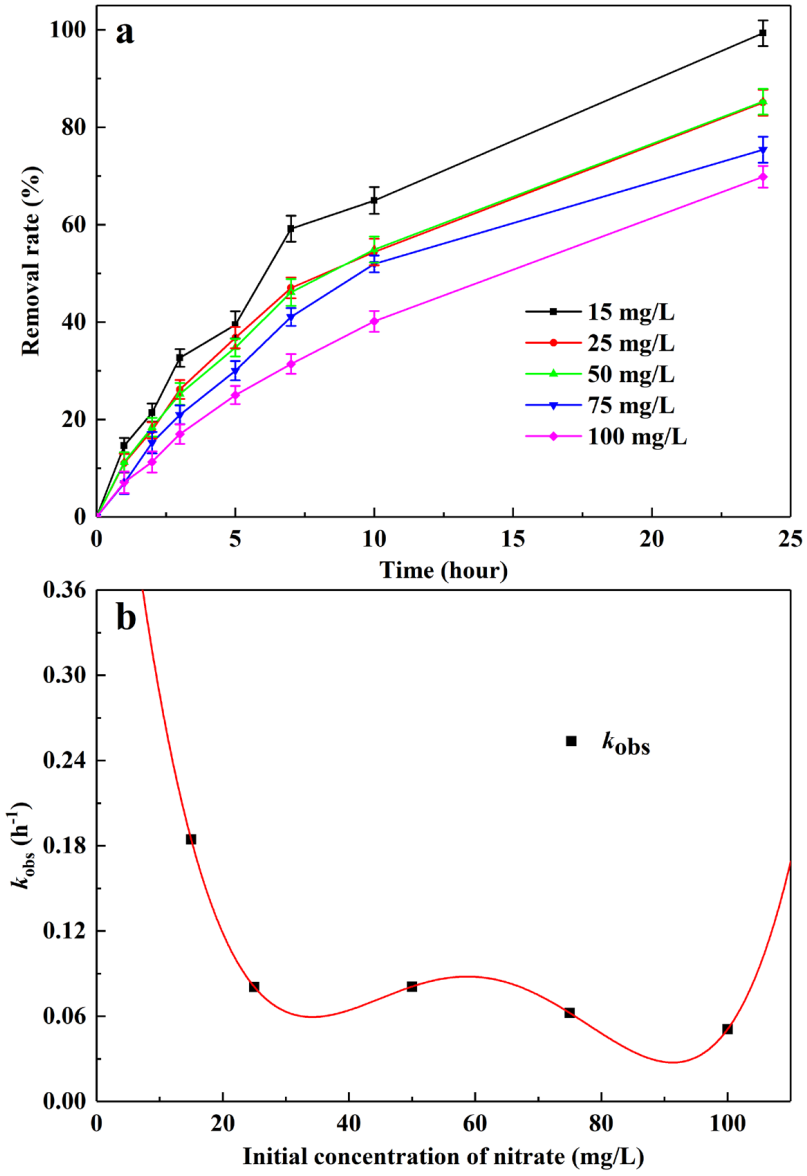

Figure 8. The denitrification performance (**a**) and k_{obs} (**b**) of nZVI/(ABS + EC) - (0.6–0.8) under different initial NO_3^--N concentrations.

Table 4. The k_{obs} (b) of nZVI/(ABS + EC) - (0.6–0.8) under different initial NO_3^--N concentrations.

No.	Initial Nitrate Concentration/(mg/L)	k_{obs}	R^2
1	15	0.1844	0.9296
2	25	0.0807	0.9938
3	50	0.0809	0.9963
4	75	0.0623	0.9759
5	100	0.0509	0.9960

In this study, k_{obs} decreased as the c_0 of NO_3^--N increased from 15 to 25 mg/L, but it increased when c_0 was greater than 100 mg/L. This phenomenon may be explained as follows. When the NO_3^--N concentration was low, the concentration of encapsulated nZVI was relatively high, and adsorption played a dominant role in the removal of NO_3^--N. Therefore, k_{obs} decreased as c_0 increased at low initial NO_3^--N concentrations. However, when the NO_3^--N concentration was high, the concentration of the encapsulated nZVI was relatively low, and reduction played a dominant role in the removal of NO_3^--N, accompanied by the generation of Fe_3O_4 and Fe^{2+} (Figure 9) [45,48,49]. Moreover, Fe^{2+} and Fe_3O_4 had prominent promotion effects on nitrate reduction and increasing the initial NO_3^--N concentration accelerated the generation of Fe_3O_4 and Fe^{2+} [45], which eventually reduced nitrate. The change in the NO_3^--N removal rate was complicated when the NO_3^--N concentration ranged from 25 to 100 mg/L, possibly due to adsorption and reduction processes. The obtained results indicate that adsorption and reduction were both involved during NO_3^--N removal, and the initial NO_3^--N concentration influenced the denitrification rate of encapsulated nZVI by adsorption and reduction.

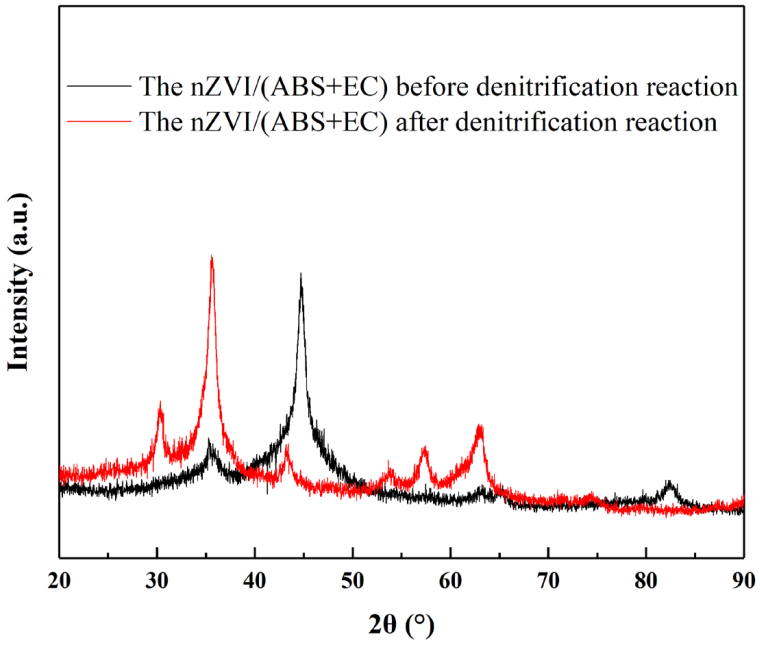

Figure 9. The XRD spectroscopy of the nZVI/(ABS + EC) - (0.6–0.8) before and after denitrification reaction under the initial NO_3^--N concentrations of 100 mg/L.

The complexity of this relationship particularly manifests within the intermediate concentration range (25 to 100 mg/L), where neither adsorption nor reduction can be solely credited for the observed denitrification performance. In conclusion, while our study has preliminarily shed light on the intricate dynamics between the initial NO_3^--N concentration and the denitrification rate of encapsulated nZVI, it also underscores the necessity for further research. To elucidate the observed complexities, a thorough and quantitative investigation of the denitrification mechanisms, taking into account factors such as pH, nZVI/(ABS + EC) concentration, and encapsulation effects, is imperative.

3.8. Effects of Reductant Concentration

The reduction of nitrate using nZVI/(ABS + EC) - (0.6–0.8) was carried out under reductant concentrations of 2 g/L, 4 g/L, 6 g/L, and 8 g/L at an initial NO_3^--N concentration of 50 mg/L at 30 °C. The denitrification performance of nZVI/(ABS + EC) - (0.6–0.8) was similar to that of nZVI, as has been previously reported [47] (Figure 10). The denitrification rate was observed to increase as the reductant concentration increased. However, the test results show that the denitrification rate rapidly increased when the reductant concentration increased from 2 g/L to 4 g/L, and then the rate increased slowly at reductant concentrations between 4 g/L and 8 g/L. These results demonstrate that the concentration of nZVI/(ABS + EC) significantly influenced the denitrification rate.

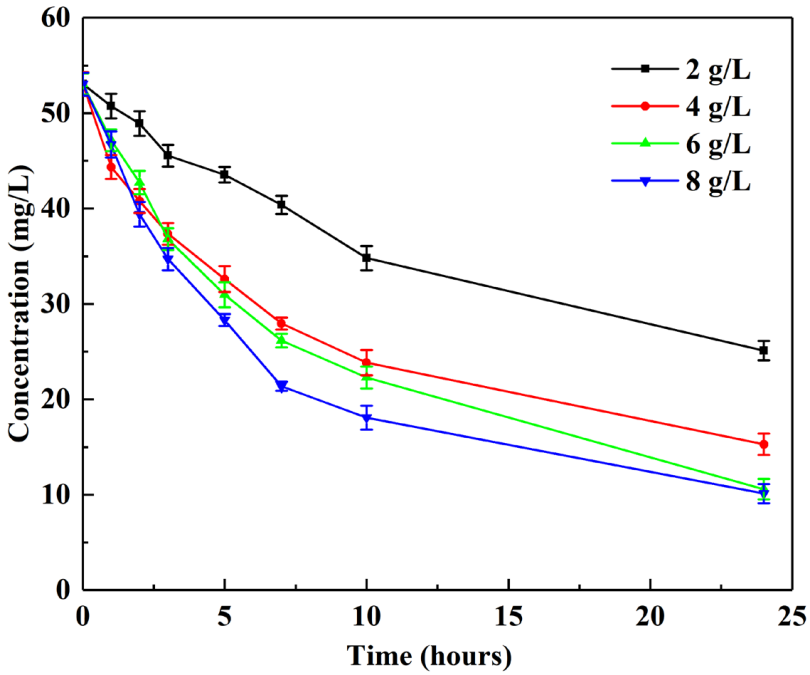

Figure 10. The denitrification performance of nZVI/(ABS + EC) - (0.6–0.8) under different reductant concentrations.

3.9. The Denitrification Mechanism of nZVI/(ABS + EC)

Previous studies have revealed that the deposition of passive iron oxides generated on the nZVI surface leads to the conglutination of nZVI particles, which would hinder the transport of electrons and transfer of mass for denitrification. Therefore, the above deposition on the nZVI particle surface can aggravate the aggregation and reactivity loss (Figure 11). For nZVI/(ABS + EC), embedding nZVI particles on a hole wall of the ABS matrix restricts the movement, thereby preventing the aggregation of nZVI particles. Moreover, the deposition of passive iron oxides generated on the ABS matrix surface, which can be confirmed in Figure 3d, can alleviate the reactivity loss. In addition, the regulation of the hole size and numbers can achieve the quantitative control of the sustainable denitrification performance, which is verified by the above result. Moreover, compared to regulating the denitrification rate of nZVI through functional group grafting modification of encapsulated shell materials [24], this study has the advantages of simple process and better controllability. That is, the encapsulation of nZVI in the ABS matrix can achieve the immobilization of nZVI particles and control the contact between the contaminant and nZVI particles, further accomplishing the anti-aggregation and control of sustainable denitrification performance of nZVI.

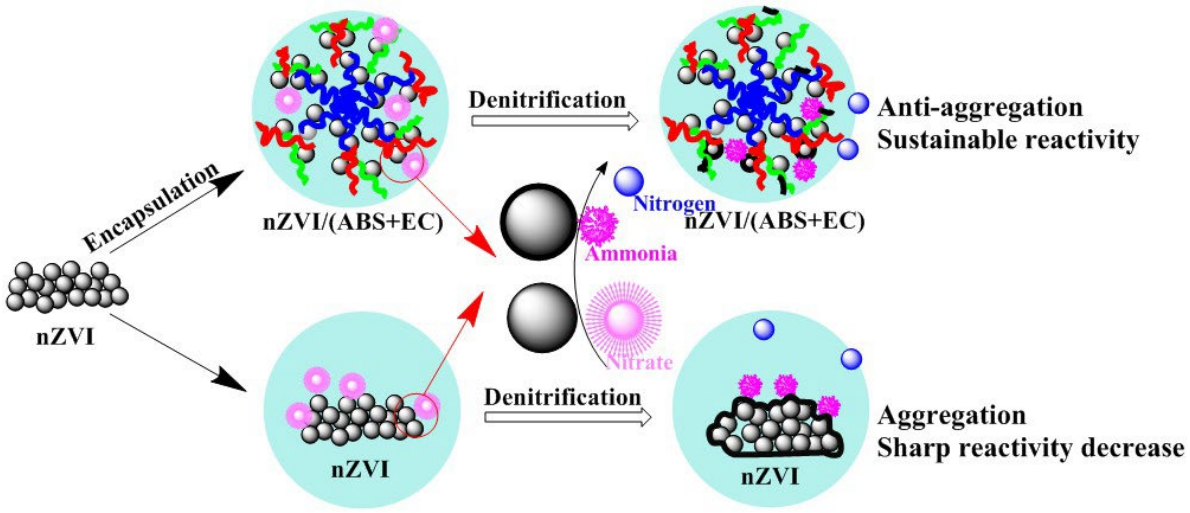

Figure 11. Denitrification mechanism of nZVI/(ABS + EC).

4. Conclusions

In this study, nZVI was successfully encapsulated in ABS for sustainable denitrification performance and anti-aggregation. The experiments demonstrated that the modification of pores within the ABS matrix using EC played a critical role in maintaining continuous nZVI reactivity. Quantitative analysis revealed a regulated denitrification rate, with apparent rate constants (k_{obs}) for denitrification performance varying from 0.0423 to 0.2036 min^{-1} across different EC and nZVI dosages. Therefore, encapsulation solves the issues of aggregation and poor reactivity persistence with the use of nZVI as the reactive medium for PRB.

Further, the denitrification rate was also affected by the pH, initial NO_3^--N concentration, and nZVI/(ABS + EC) concentration. A particularly interesting observation was the dependence of the observed rate constant (k_{obs}) on the initial NO_3^--N concentration, which was meticulously analyzed through first-order kinetic modeling. The study revealed that at varying initial NO_3^--N concentrations, the denitrification mechanism of nZVI/(ABS + EC) exhibited complex behavior, underscoring the intertwined roles of adsorption and reduction processes in NO_3^--N removal. However, the denitrification mechanism of nZVI must be thoroughly and quantitatively examined to precisely explain the observed complicated denitrification performance of nZVI/(ABS + EC) under the experimental conditions in this study. Moreover, for a comprehensive understanding of the economic efficiency of nZVI/(ABS + EC) for denitrification, future work will explore a detailed cost–benefit analysis, considering factors such as long-term operation, maintenance, and potential scalability of the nZVI/(ABS + EC) system for widespread environmental remediation applications.

Author Contributions: Conceptualization, F.M.; Methodology, M.L.; Formal analysis, Q.Z.; Investigation, Y.Y.; Data curation, C.Y.; Writing—original draft, F.M.; Supervision, B.Q.; Project administration, F.M.; Funding acquisition, F.M. All authors have read and agreed to the published version of the manuscript.

Funding: This research was funded by National Natural Science Foundation of China [grant number 42207083].

Data Availability Statement: Data are contained within the article.

Conflicts of Interest: All authors except Miao Li was employed by the company "SINOPEC Research Institute of Petroleum Processing Co., Ltd.". Miao Li declares that the research was conducted in the absence of any commercial or financial relationships that could be construed as a potential conflict of interest.

References

1. Bahrami, F.; Yu, X.; Zou, Y.; Sun, Y.; Sun, G. Impregnated calcium-alginate beads as floating reactors for the remediation of nitrate-contaminated groundwater. *Chem. Eng. J.* **2020**, *382*, 122774. [CrossRef]
2. Wakida, F.T.; Lerner, D.N. Non-agricultural sources of groundwater nitrate: A review and case study. *Water Res.* **2005**, *39*, 3–16. [CrossRef] [PubMed]
3. Hamad, J.R.J.; Yaacob, W.Z.; Omran, A. Quality Assessment of Groundwater Resources in the City of Al-Marj, Libya. *Processes* **2021**, *9*, 154. [CrossRef]
4. Suthar, S.; Bishnoi, P.; Singh, S.; Mutiyar, P.K.; Nema, A.K.; Patil, N.S. Nitrate contamination in groundwater of some rural areas of Rajasthan, India. *J. Hazard. Mater.* **2009**, *171*, 189–199. [CrossRef] [PubMed]
5. Rivett, M.O.; Buss, S.R.; Morgan, P.; Smith, J.W.N.; Bemment, C.D. Nitrate attenuation in groundwater: A review of biogeochemical controlling processes. *Water Res.* **2008**, *42*, 4215–4232. [CrossRef] [PubMed]
6. Huang, C.; Wang, H.; Chiu, P. Nitrate reduction by metallic iron. *Water Res.* **1998**, *32*, 2257–2264. [CrossRef]
7. Ruhl, A.S.; Jekel, M. Impacts of Fe(0) grain sizes and grain size distributions in permeable reactive barriers. *Chem. Eng. J.* **2012**, *213*, 245–250. [CrossRef]
8. Fu, F.; Dionysiou, D.D.; Liu, H. The use of zero-valent iron for groundwater remediation and wastewater treatment: A review. *J. Hazard. Mater.* **2014**, *267*, 194–205. [CrossRef] [PubMed]
9. Zarime, N.A.; Solemon, B.; Wan Yaacob, W.Z.; Jamil, H.; Che Omar, R.; Rafek, A.G.; Roslan, R. Adsorption of Methylene Blue by Bentonite Supported Nano Zero Valent Iron (B-nZVI). *Processes* **2023**, *11*, 788. [CrossRef]
10. Yang, G.C.C.; Lee, H. Chemical reduction of nitrate by nanosized iron: Kinetics and pathways. *Water Res.* **2005**, *39*, 884–894. [CrossRef]
11. Abdelfatah, A.M.; Fawzy, M.; Eltaweil, A.S.; El-Khouly, M.E. Green Synthesis of Nano-Zero-Valent Iron Using Ricinus Communis Seeds Extract: Characterization and Application in the Treatment of Methylene Blue-Polluted Water. *ACS Omega* **2021**, *6*, 25397–25411. [CrossRef] [PubMed]
12. Huang, T.; Liu, L.; Zhang, S.; Xu, J. Evaluation of electrokinetics coupled with a reactive barrier of activated carbon loaded with a nanoscale zero-valent iron for selenite removal from contaminated soils. *J. Hazard. Mater.* **2019**, *368*, 104–114. [CrossRef] [PubMed]
13. Maamoun, I.; Eljamal, O.; Khalil, A.M.E.; Sugihara, Y.; Matsunaga, N. Phosphate Removal Through Nano-Zero-Valent Iron Permeable Reactive Barrier; Column Experiment and Reactive Solute Transport Modeling. *Transp. Porous Med.* **2018**, *125*, 395–412. [CrossRef]
14. Tosco, T.; Petrangeli Papini, M.; Cruz Viggi, C.; Sethi, R. Nanoscale zerovalent iron particles for groundwater remediation: A review. *J. Clean. Prod.* **2014**, *77*, 10–21. [CrossRef]
15. Shao, Y.; Gao, Y.; Yue, Q.; Kong, W.; Gao, B.; Wang, W.; Jiang, W. Degradation of chlortetracycline with simultaneous removal of copper (II) from aqueous solution using wheat straw-supported nanoscale zero-valent iron. *Chem. Eng. J.* **2020**, *379*, 122384. [CrossRef]
16. Eltaweil, A.S.; El-Tawil, A.M.; Abd El-Monaem, E.M.; El-Subruiti, G.M. Zero Valent Iron Nanoparticle-Loaded Nanobentonite Intercalated Carboxymethyl Chitosan for Efficient Removal of Both Anionic and Cationic Dyes. *ACS Omega* **2021**, *6*, 6348–6360. [CrossRef] [PubMed]
17. Ruiz-Torres, C.A.; Araujo-Martínez, R.F.; Martínez-Castañón, G.A.; Morales-Sánchez, J.E.; Guajardo-Pacheco, J.M.; González-Hernández, J.; Lee, T.; Shin, H.; Hwang, Y.; Ruiz, F. Preparation of air stable nanoscale zero valent iron functionalized by ethylene glycol without inert condition. *Chem. Eng. J.* **2018**, *336*, 112–122. [CrossRef]
18. Zhang, J.; Zhang, G.; Zheng, K.; Cai, D.; Wu, Z. Reduction of Cr (VI) by urea-dispersed nanoscale zero-valent iron. *J. Nanosci. Nanotechnol.* **2015**, *15*, 6103–6107. [CrossRef] [PubMed]
19. Zhang, J.; Zhang, G.; Wang, M.; Zheng, K.; Cai, D.; Wu, Z. Reduction of aqueous Cr VI using nanoscale zero-valent iron dispersed by high energy electron beam irradiation. *Nanoscale* **2013**, *5*, 9917–9923. [CrossRef] [PubMed]
20. Fan, D.; O'Carroll, D.M.; Elliott, D.W.; Xiong, Z.; Tratnyek, P.G.; Johnson, R.L.; Garcia, A.N. Selectivity of nano zerovalent iron in in situ chemical reduction: Challenges and improvements. *Remediat. J.* **2016**, *26*, 27–40. [CrossRef]
21. O'Connor, D.; Hou, D.; Ok, Y.S.; Song, Y.; Sarmah, A.; Li, X.; Tack, F.M. Sustainable in situ remediation of recalcitrant organic pollutants in groundwater with controlled release materials: A review. *J. Control. Release* **2018**, *283*, 200–213. [CrossRef] [PubMed]
22. Matlochová, A.; Plachá, D.; Rapantová, N. The application of nanoscale materials in groundwater remediation. *Pol. J. Environ. Stud.* **2013**, *22*, 1401–1410.
23. Karimi, B.; Samadi, S. Nitrate removal from aqueous solution: Using zero-valent iron (Fe degrees) fixed on Ca-alginate bead. *Desalin. Water Treat.* **2019**, *143*, 235–239. [CrossRef]
24. Krajangpan, S.; Bermudez, J.J.E.; Bezbaruah, A.N.; Chisholm, B.J.; Khan, E. Nitrate removal by entrapped zero-valent iron nanoparticles in calcium alginate. *Water Sci. Technol.* **2008**, *58*, 2215–2222. [CrossRef] [PubMed]
25. Jiang, Z.; Lv, L.; Zhang, W.; Du, Q.; Pan, B.; Yang, L.; Zhang, Q. Nitrate reduction using nanosized zero-valent iron supported by polystyrene resins: Role of surface functional groups. *Water Res.* **2011**, *45*, 2191–2198. [CrossRef] [PubMed]
26. Wang, X.; Zhang, B.; Ma, J.; Ning, P. Chitosan Modifying Nanoscale Zero Valent Iron for Tetracycline Removal from Aqueous Solutions: Proposed Pathway. *Environ. Eng. Sci.* **2019**, *36*, 273–282. [CrossRef]

27. Choi, H.; Al-Abed, S.R.; Agarwal, S. Effects of aging and oxidation of palladized iron embedded in activated carbon on the dechlorination of 2-chlorobiphenyl. *Environ. Sci. Technol.* **2009**, *43*, 4137–4142. [CrossRef] [PubMed]
28. Wang, X.; Yi, D.; Ma, J. Novel synthesis of carbon spheres supported nanoscale zero-valent iron for removal of metronidazole. *Appl. Surf. Sci.* **2016**, *390*, 50–59. [CrossRef]
29. Su, C.; Puls, R.W.; Krug, T.A.; Watling, M.T.; O'Hara, S.K.; Quinn, J.W.; Ruiz, N.E. A two and half-year-performance evaluation of a field test on treatment of source zone tetrachloroethene and its chlorinated daughter products using emulsified zero valent iron nanoparticles. *Water Res.* **2012**, *46*, 5071–5084. [CrossRef]
30. Ferrari, P.F.; Trucillo, P.; De Negri Atanasio, G.; Bufalini, C.; Campardelli, R.; Perego, P.; Palombo, D.; Reverchon, E. Operating Parameters Optimization for the Production of Liposomes Loaded with Antibodies Using a Supercritical Fluid-Assisted Process. *Processes* **2023**, *11*, 663. [CrossRef]
31. Mora-Huertas, C.E.; Fessi, H.; Elaissari, A. Polymer-based nanocapsules for drug delivery. *Int. J. Pharmaceut.* **2010**, *385*, 113–142. [CrossRef] [PubMed]
32. Guan, H.; Chi, D.; Yu, J.; Li, H. Encapsulated ecdysone by internal gelation of alginate microspheres for controlling its release and photostability. *Chem. Eng. J.* **2011**, *168*, 94–101. [CrossRef]
33. Gonzalez Gomez, A.; Syed, S.; Marshall, K.; Hosseinidoust, Z. Liposomal Nanovesicles for Efficient Encapsulation of Staphylococcal Antibiotics. *ACS Omega* **2019**, *4*, 10866–10876. [CrossRef]
34. Kavetsou, E.; Koutsoukos, S.; Daferera, D.; Polissiou, M.G.; Karagiannis, D.; Perdikis, D.; Detsi, A. Encapsulation of Mentha pulegium essential oil in yeast cell microcarriers: An approach to environmentally friendly pesticides. *J. Agric. Food Chem.* **2019**, *67*, 4746–4753. [CrossRef]
35. Lin, G.; Chen, X.; Zhou, H.; Zhou, X.; Xu, H.; Chen, H. Elaboration of a feather keratin/carboxymethyl cellulose complex exhibiting pH sensitivity for sustained pesticide release. *J. Appl. Polym. Sci.* **2019**, *136*, 47160. [CrossRef]
36. Slattery, M.; Harper, B.; Harper, S. Pesticide Encapsulation at the Nanoscale Drives Changes to the Hydrophobic Partitioning and Toxicity of an Active Ingredient. *Nanomaterials* **2019**, *9*, 81. [CrossRef]
37. Maes, C.; Menot, B.; Hayouni, S.; Martinez, A.; Fauconnier, M.; Bouquillon, S. Preparation of New Glycerol-Based Dendrimers and Studies on Their Behavior toward Essential Oil Encapsulation. *ACS Omega* **2022**, *7*, 10277–10291. [CrossRef] [PubMed]
38. Fugolin, A.P.P.; Ferracane, J.L.; Pfeifer, C.S. Fatigue-Crack Propagation Behavior in Microcapsule-Containing Self-Healing Polymeric Networks. *Mater. Des.* **2022**, *223*, 111142. [CrossRef]
39. Gharsallaoui, A.; Roudaut, G.; Chambin, O.; Voilley, A.; Saurel, R. Applications of spray-drying in microencapsulation of food ingredients: An overview. *Food Res. Int.* **2007**, *40*, 1107–1121. [CrossRef]
40. Augustin, M.A.; Hemar, Y. Nano-and micro-structured assemblies for encapsulation of food ingredients. *Chem. Soc. Rev.* **2009**, *38*, 902–912. [CrossRef] [PubMed]
41. Rubio-Rodríguez, N.; Beltrán, S.; Jaime, I.; Sara, M.; Sanz, M.T.; Carballido, J.R. Production of omega-3 polyunsaturated fatty acid concentrates: A review. *Innov. Food Sci. Emerg.* **2010**, *11*, 1–12. [CrossRef]
42. Paulo, F.; Santos, L. Design of experiments for microencapsulation applications: A review. *Mater. Sci. Eng. C* **2017**, *77*, 1327–1340. [CrossRef] [PubMed]
43. Meng, F.; Wang, S.; Liu, H.; Xu, X.; Ma, H. Microencapsulation of oxalic acid (OA) via coacervation induced by polydimethylsiloxane (PDMS) for the sustained release performance. *Mater. Des.* **2017**, *116*, 31–41. [CrossRef]
44. Meng, F.; Li, M.; Wang, S.; Liu, X.; Gao, W.; Ma, Z.; Kong, C.; Ma, X.; Li, J. Encapsulation of potassium persulfate with ABS via coacervation for delaying the viscosity loss of fracturing fluid. *J. Appl. Polym. Sci.* **2019**, *136*, 47734. [CrossRef]
45. Xu, J.; Hao, Z.; Xie, C.; Lv, X.; Yang, Y.; Xu, X. Promotion effect of Fe^{2+} and Fe_3O_4 on nitrate reduction using zero-valent iron. *Desalination* **2012**, *284*, 9–13. [CrossRef]
46. Wang, W.; Jin, Z.; Li, T.; Zhang, H.; Gao, S. Preparation of spherical iron nanoclusters in ethanol–water solution for nitrate removal. *Chemosphere* **2006**, *65*, 1396–1404. [CrossRef] [PubMed]
47. Zhang, J.; Hao, Z.; Zhang, Z.; Yang, Y.; Xu, X. Kinetics of nitrate reductive denitrification by nanoscale zero-valent iron. *Process Saf. Environ.* **2010**, *88*, 439–445. [CrossRef]
48. Suzuki, T.; Moribe, M.; Oyama, Y.; Niinae, M. Mechanism of nitrate reduction by zero-valent iron: Equilibrium and kinetics studies. *Chem. Eng. J.* **2012**, *183*, 271–277. [CrossRef]
49. Noubactep, C. Comments on 'Mechanism study of nitrate reduction by nano zero valent iron' by Hwang et al. [J. Hazard. Mater. (2010). https://doi.org/10.1016/j.jhazmat.2010.10.078]. *J. Hazard. Mater.* **2011**, *186*, 946–947. [CrossRef] [PubMed]